



LAWRENCE
LIVERMORE
NATIONAL
LABORATORY

A Model of Plasma Rotation in the Livermore Spheromak for the Regimes of Large Connection Lengths

D.D. Ryutov

January 4, 2007

Physics of Plasmas

Disclaimer

This document was prepared as an account of work sponsored by an agency of the United States Government. Neither the United States Government nor the University of California nor any of their employees, makes any warranty, express or implied, or assumes any legal liability or responsibility for the accuracy, completeness, or usefulness of any information, apparatus, product, or process disclosed, or represents that its use would not infringe privately owned rights. Reference herein to any specific commercial product, process, or service by trade name, trademark, manufacturer, or otherwise, does not necessarily constitute or imply its endorsement, recommendation, or favoring by the United States Government or the University of California. The views and opinions of authors expressed herein do not necessarily state or reflect those of the United States Government or the University of California, and shall not be used for advertising or product endorsement purposes.

A model of plasma rotation in the Livermore spheromak for the regimes of large connection lengths

D.D. Ryutov

Lawrence Livermore National Laboratory, Livermore, CA 94551

ABSTRACT

A model is suggested that predicts the velocity and geometrical characteristics of the plasma rotation in the Livermore spheromak. The model addresses the “good confinement” regimes in this device, where the typical length of magnetic field lines before their intersection with the wall (this length is called “connection length” below) becomes large enough to make the parallel heat loss insignificant. In such regimes, the heat flux is determined by the transport across toroidally-averaged flux surfaces. The model is based on the assumption that, entering the good confinement regime, does not automatically mean that the connection length becomes infinite, and perfect flux surfaces are established. It is hypothesized that connection length remains finite, albeit large in regard to the parallel heat loss. The field lines are threading the whole plasma volume, although it takes a long distance for them to get from one toroidally-averaged flux surface to another. The parallel electron momentum balance then uniquely determines the distribution of the electrostatic potential between these surfaces. An analysis of viscous stresses shows that the toroidal flow is much faster than the poloidal flow. It is shown that the rotation shear usually exceeds by a factor of a few the characteristic growth rate of drift waves, meaning that suppression of the transport caused by the drift turbulence may occur, and a transport barrier with respect to this transport mechanism may be formed. The model may be useful for assessing the plasma rotation in other spheromaks and, possibly, reversed-field pinches and field-reversed configurations, provided a certain set of applicability conditions (Sec. II) is fulfilled.

PACS Numbers: 52.55.Ip; 52.55.Hc; 52.30.-q

ryutov1@llnl.gov

I. INTRODUCTION

The spheromak is an extreme example of a magnetically self-organized toroidal system, where the conversion of the poloidal to the toroidal current occurs via the magnetic reconnection process [1,2]. This process, generally speaking, leads to the magnetic field lines stochastization. In the regime of spheromak formation, early in the pulse, where the reconnection process is active and the system is far from the relaxed Taylor-like state, the field lines between their intersection with the walls of the vacuum chamber are short, and the confinement is dominated by the heat loss along the field lines. However, when a state close to a relaxed state is formed, the magnetic fluctuations decrease, and the field line length becomes so large that the cross-field heat transport takes over the parallel transport. In this regime, electron temperature and density become approximately constant over flux surfaces of the toroidally-averaged magnetic field (we will use a shorter term “toroidally-averaged flux surfaces” and an acronym “TAFS” throughout the paper), and this is a regime that we are going to study in this paper.

The aforementioned transition has been identified both experimentally [3] and in numerical simulations [4, 5]. The parallel confinement time for a poor confinement regime was evaluated in Refs. [6,7]. The statistics of the field line lengths was studied in Refs. [8, 9].

Leaving the detailed discussion of the model used in this paper until Sec. II, here we just mention our key hypothesis, which is that transition to the good confinement does not mean the flux surfaces suddenly become perfect. We hypothesize that even in the regime of a good confinement they remain “fuzzy”, and the plasma interior remains connected to the cold external plasma along the field lines, albeit the connection length

becomes very large. The analysis of the electron parallel momentum balance then shows that the plasma potential is constant over TAFS, meaning that toroidal rotation frequency is constant over TAFS (Secs. III, IV). All these predictions could be verified experimentally. The rotation frequency, generally speaking, varies from one flux surface to another, i.e., the rotation shear is present. The rotation shear may be large and may lead to the suppression of the drift-wave turbulence and, possibly, to the formation of transport barriers with respect to the drift transport.

We concentrate on the parameter domain typical for the Livermore spheromak SSPX (Sustained Spheromak Physics Experiment), although our analysis may be applicable to other devices, provided that applicability conditions specified in Sec. II are satisfied. A rough schematic of TAFS in SSPX is shown in Fig. 1. As a characteristic set of parameters, we take the ones presented in Table 1 based on Refs. [3, 10, 11]. The following notation is used in TABLE 1 and throughout the paper: R_θ is the distance between the geometrical and magnetic axis, a_S is characteristic “radius” of the last closed flux surface, n , T_e , and Z_{eff} are the density, electron temperature and the parameter characterizing the presence of higher- Z ions, respectively, B_T and B_P are the toroidal and poloidal magnetic field strengths near the outer wall. In the Table, we cite some “characteristic” electron temperature, averaged over the confinement volume; the maximum temperature was approximately 350 eV [10, 11].

In TABLE 2, we present some relevant derived parameters corresponding to the numbers mentioned in TABLE 1. The following notation is used: ν_{ei} is the electron-ion collision frequency, λ_{ei} is the electron-ion collision length, N is a number of mean free

paths over the toroidal circumference, $c_s \equiv \sqrt{2T_e/m_i}$, and ρ_i^* is the ion gyroradius evaluated for the electron temperature, $\rho_i^* = c_s/\omega_{Ci}$.

II. THE MODEL

We consider regimes of a good confinement, where the characteristic field line connection length L (which we define as a characteristic distance along the field line between a point in the plasma interior and the separatrix) becomes so large that the parallel heat loss becomes negligible. At the same time, we hypothesize that this length still remains finite (albeit large) so that any point inside the plasma still remains connected to the cold plasma near the separatrix. This is a hypothesis, not a proven fact. But we believe that transition from a poor to a good confinement is gradual, so that the parameter L does not jump from some large value to infinity in the form similar to the phase transition. We analyze the consequences of this hypothesis and come up with predictions regarding the plasma rotation that can be verified experimentally, thereby proving or disproving the main hypothesis.

Note that there are no rotation measurements in good confinement regimes of SSPX experiment. There are some indirect indications that the rotation may be present. In particular, in order to make magnetic fluctuation spectra consistent with experimental spectra, a rotation with a frequency $f=20$ kHz was imposed in the numerical simulations of SSPX [5]. As we shall see, this frequency is consistent with our model, although there is no way for a more detailed comparison at present. Rotation at the formation phase may also be present (see Refs. [12, 13] and references therein), but our model cannot be applied to this case because of a short connection length during the formation phase. We

also note that in the NIMROD simulations [9], a slow rotation of the modes was observed when two-fluid effects were included.

Small magnetic fluctuations and the large connection length mean that the field line makes many revolutions in toroidal and poloidal directions before it goes far away from the flux surface where it has originated from. This means that the electron temperature will be constant over the flux surface. The plasma density will also equalize over the flux surface.

The main point of our hypothesis is that the plasma interiors still remain connected to the periphery, although connection length is large, so that the time for establishing the temperature equilibrium along the field line is large compared to the time of cross-field loss. The heat balance equation can be schematically presented as:

$$\frac{3}{2} n \frac{dT_e}{dt} = -\frac{3 n T_e}{2 \tau_{\parallel}} - \frac{3 n T_e}{2 \tau_{\perp}} + Q_J, \quad (1)$$

where the first term in the right hand side (RHS) describes the parallel heat loss, with τ_{\parallel} being the heat conduction time proportional to L^2 , the second term relates to the perpendicular heat conduction, and Q_J is the heat source (predominantly Joule heating for the conditions of SSPX experiment). As mentioned, at large-enough L , the condition $\tau_{\parallel} > \tau_{\perp}$ would be met, and the first term in the RHS would become negligible, meaning that in the quasi-steady state the temperature would vary according to the balance of the second from the last and the last term. This can also be formulated as the following statement: the time for establishing the parallel heat balance is much greater than the experimental confinement time. The radial temperature profile will be established as a result of balancing heat sources and cross-field diffusion. We do not need to specify the mechanism of the cross-field energy loss, be it the anomalous transport associated with

drift-wave (or other) microturbulence, or, as an extreme case, a classical ion thermal conduction. What we need, is just the experimental estimate of the confinement time τ_{\perp} .

The parallel confinement time can be roughly evaluated as (Cf. Refs. [6,7])

$$\tau_{\parallel} \sim \frac{L^2}{4\lambda_{ei}v_{Te}}, \quad (2)$$

or, in “practical” units

$$\tau_{\parallel}(s) \sim 10^{-21} \frac{Z_{eff} [L(cm)]^2 n(cm^{-3})}{[T_e(eV)]^{5/2}}. \quad (3)$$

According to Eq. (2), the condition $\tau_{\parallel} > \tau_{\perp}$ is met for L exceeding some critical length L_1 ,

$$L > L_1 \equiv 2\sqrt{\lambda_{ei}v_{Te}\tau_{\perp}}. \quad (4)$$

For the “characteristic” regime described by Table 1, this condition is met for $L > 100$ m.

The absence of the parallel thermal equilibrium does not mean that there is no mechanical equilibrium of the electron gas along the field line. Indeed, the parallel momentum equation for the electrons is [14]:

$$mn \frac{dv_{\parallel}}{dt} = -\frac{\partial(nT_e)}{\partial s} - 0.71n \frac{\partial T_e}{\partial s} + en \frac{\partial \varphi}{\partial s} \quad (5)$$

and, because of a small electron mass, the inertial term in the left-hand side (LHS) can be neglected (compared to, say, pressure term in the RHS) for not-too-large connection lengths. Indeed, relating the change of the plasma parameters along the flux tubes to the time τ_{\perp} , one can write this condition as

$$\frac{mnL}{\tau_{\perp}^2} < \frac{nT_e}{L}, \quad (6)$$

or

$$L < L_2 \equiv v_{Te}\tau_{\perp}. \quad (7)$$

The meaning of the other terms in the RHS of Eq. (5) is as follows [14]: the second term describes the thermal force acting on the electrons, and the third term is the effect of a static electric field. The numerical coefficient 0.71 in front of the thermal force corresponds to a purely hydrogen plasma; it is slightly larger for the plasma with $Z_{eff}=2$, but we neglect this difference. Strictly speaking, one should have added two more terms to the RHS of Eq. (5): the friction force caused by the presence of a parallel current, $m_e \nu_{ei} j_{\parallel} / e$, and the electric force $-enE_{\parallel}$ caused by the vortex electric field that drives this current. However, these two forces cancel each other, $m_e \nu_{ei} j_{\parallel} / e - enE_{\parallel} = 0$, and do not contribute to the momentum balance, Eq. (5).

For the parameters of Table 1, L_2 is 2000 m, i.e., much greater than L_1 (Eq. (4)). In other words, field lines may be long enough so that the parallel thermal equilibrium is absent, but the parallel mechanical equilibrium is present. This is exactly the regime for which our model should work.

In this regime, the plasma temperature and density are, to a high accuracy, constant over TAFS; on the other hand, every point inside the plasma is still connected to the vicinity of the wall, just the connection length is large. This is a regime which we assess in the rest of the paper.

III. POTENTIAL DISTRIBUTION INSIDE THE PLASMA

Denoting by Ψ the poloidal magnetic flux enclosed by some flux surface (we measure Ψ from the magnetic axis where it is zero), one can state that $T_e = T_e(\Psi)$, $n = n(\Psi)$. This simultaneously means that one can consider the temperature as a function of density, $T_e = T_e(n)$. [If the density is a non-monotonic function of the flux, this dependence may have more than one branch, but this does not change anything

substantial in the further analysis.] With this observation in mind, one can rewrite Eq. (5)

as:

$$e \frac{\partial \varphi}{\partial s} = \frac{\partial}{\partial s} \left[\int_{n_s}^n \frac{dn}{n T_e^{0.71}} \frac{d}{dn} (n T_e^{1.71}) \right] \quad (8)$$

where n_s is the density in the vicinity of the separatrix (which, in the case of SSPX, is very close to the wall). Integrating this equation from the separatrix to the plasma core, we find:

$$\varphi = \varphi_s + \frac{1}{e} \int_{n_s}^n \frac{dn}{n T_e^{0.71}} \frac{d}{dn} (n T_e^{1.71}) \quad (9)$$

The plasma at the separatrix and outside it is much colder than the plasma in the core, and the potential variation in this zone is also small. So, we neglect the term φ_s in Eq. (9) and obtain:

$$\varphi \approx \frac{1}{e} \int_{n_s}^n \frac{dn}{n T_e^{0.71}} \frac{d}{dn} (n T_e^{1.71}) \quad (10)$$

As n and T_e are the flux functions, so is the electrostatic potential determined from Eq. (10). In other words, according to this analysis, the potential is constant over each flux surface. This, in particular, means that the electric field has only a normal (to the flux surface) component E_n . The normal distance between two flux surfaces separated by the flux $\Delta\Psi$ is $\Delta\Psi/2\pi R B_p$, where R is the major radius of the observation point and B_p is the magnetic field at this point. Accordingly, E_n can be evaluated as:

$$E_n = -2\pi R B_p \frac{\partial \varphi}{\partial \Psi} = -\frac{2\pi R B_p}{e} \frac{\partial}{\partial \Psi} \left[\int_{n_s}^n \frac{dn}{n T_e^{0.71}} \frac{d}{dn} (n T_e^{1.71}) \right] = -\frac{2\pi R B_p}{e} \left(\frac{T_e}{n} \frac{\partial n}{\partial \Psi} + 1.71 \frac{\partial T_e}{\partial \Psi} \right). \quad (11)$$

IV. EVALUATION OF THE ROTATION VELOCITY

To find the rotation velocity in the presence of the electric field normal to the flux surfaces, we consider three components of the momentum equation for the ion guiding centers. The normal component is:

$$e \left(E_n - \frac{1}{c} v_T B_p + \frac{1}{c} v_p B_T \right) = 0 \quad (12)$$

We assume that the ions are colder than electrons, $T_i < T_e$, and neglect the $\text{grad}B$ force and the centrifugal force in this equation. Their ratio to the first term in the l.h.s. is $\sim T_i/T_e$. The assumption $T_i < T_e$, may have a justification in the SSPX case, where the dominant heating mechanism in the quiescent, good confinement mode, is Joule heating, which predominantly heats electrons. We will discuss possible changes in our predictions for the $T_i \sim T_e$ case in Sec. VI.

The toroidal component is:

$$\frac{1}{c} v_n B_p + f_T^{(visc)} = 0, \quad (13)$$

where $f_T^{(visc)} \sim m_i \eta_{\perp} v_T / a^2$ is a viscous force caused by the possible shearing of the toroidal flow, with $\eta_{\perp} \sim \rho_i^2 \nu_{ii}$ being a shear kinematic viscosity [14]. Here ρ_i is the ion gyro-radius, and ν_{ii} is the ion-ion collision frequency.

The poloidal component is:

$$-\frac{1}{c} v_n B_T + f_p^{(visc)} = 0, \quad (14)$$

with $f_p^{(visc)} \sim m_i \eta_{\parallel} v_p / a^2$ being the poloidal viscous force, and $\eta_{\parallel} \sim \lambda_i^2 \nu_{ii}$ being the parallel kinematic viscosity [14]. Here λ_i is the ion-ion mean free path. The parallel viscosity comes into play due to the fact that, in such a tight-aspect-ratio system as the spheromak

is, the continuity of the poloidal flow leads to an order-of-one variation of the poloidal velocity over the flux surface.

By noting that, in a spheromak, the poloidal and toroidal components of the magnetic field are of the same order of magnitude, $B_p \sim B_T$, and eliminating v_n from Eqs (13) and (14), one finds that $f_p^{(visc)}/f_T^{(visc)} \sim 1$ and, accordingly, $v_p \sim (\rho_i/\lambda_i)^2 v_T \ll v_T$. In other words, one can expect that the poloidal velocity in a spheromak will be much less than the toroidal velocity. Then, neglecting the poloidal velocity in Eq. (12), one finds the following simple expression for the toroidal velocity:

$$v_T = c \frac{E_n}{B_p} = -\frac{2\pi c R}{e} \frac{\partial}{\partial \Psi} \left[\int_{n_s}^n \frac{dn}{n T_e^{0.71}} \frac{d}{dn} (n T_e^{1.71}) \right] = -\frac{2\pi c R}{e n T_e^{0.71}} \frac{\partial}{\partial \Psi} (n T_e^{1.71}) \quad (15)$$

We have used Eq. (11) for the electric field. There is no singularity in the toroidal velocity at the magnetic axis.

The angular frequency of the toroidal rotation, $\Omega \equiv v_T/R$, is equal to:

$$\Omega = -\frac{2\pi c}{e} \frac{\partial}{\partial \Psi} \left[\int_{n_s}^n \frac{dn}{n T_e^{0.71}} \frac{d}{dn} (n T_e^{1.71}) \right] = -\frac{2\pi c}{e n T_e^{0.71}} \frac{\partial}{\partial \Psi} (n T_e^{1.71}) \quad (16)$$

The rotation frequency is a flux function, i.e., it is constant at any given flux surface; on the other hand, it may vary from one flux-surface to another, i.e., a shear in the toroidal rotation may be present. The velocity shear can be characterized by the quantity of the dimension of frequency,

$$\omega = 2\pi B_p R^2 \frac{\partial \Omega}{\partial \Psi} \quad (17)$$

One can check that, for the function $n T_e^{1.71}$ monotonically decreasing in the radial direction, the rotation occurs in the direction of the toroidal current. By the order of magnitude, the rotation velocity is $c_s \rho_i^*/a_s$, where $c_s = (2T_e/m_i)^{1/2}$ is the ion sound

velocity, and $\rho_i^* = c_s/\omega_{ci}$. In other words, the flow is deeply sub-sonic and does not have any significant influence on the plasma equilibrium.

V. SIMPLE EXAMPLES

A. Potential distribution

Eqs. (10) and (16) allow one to find the radial distribution of the electrostatic potential and rotation frequency for the known distributions of the density and electron temperature. In order to have some general idea of the possible results and in order to have simple analytic expressions suitable for quick scoping analyses, we consider the simplest possible model of the plasma, where the spheromak is “rectified” in the toroidal direction, to form a periodic cylinder, with the axial period $2\pi R_\theta$, where R_θ is the radius of the magnetic axis in a real spheromak (Fig. 1). We further assume that the flux surfaces are just nested concentric circles. We will then associate the rotation frequency with v_T/R_θ . The toroidal current density will be assumed to be uniform, meaning that the poloidal magnetic field scales as

$$B_p = B_{PS} \frac{r}{a_s} \quad (18)$$

where r is the distance from the magnetic axis, a_s is a radius that would mark the location of a separatrix in a real geometry, and B_{PS} is the magnetic field at this radius. This is, of course, a very crude model, but still sufficient to make order-of-magnitude estimates and identify some trends.

The radial dependences of the electron temperature and plasma density will be parametrized as

$$T_e = T_{e0} \exp\left(-\frac{r^2}{a_T^2}\right); \quad n = n_0 \exp\left(-\frac{r^2}{a_n^2}\right), \quad (19)$$

where subscript “0” designates the quantities at the magnetic axis, and the parameters a_T and a_n are length-scales of the radial variation of the temperature and density. They are related to the values of T_e and n at the outermost flux surface $r=a_S$:

$$a_T^2 = a_S^2 / \ln(T_{e0} / T_{eS}); \quad a_n^2 = a_S^2 / \ln(n_0 / n_S). \quad (20)$$

Using these equation and Eq. (10), one finds:

$$\varphi = \frac{\ln(n_0 / n_S) + 1.71 \cdot \ln(T_{e0} / T_{eS})}{\ln(T_{e0} / T_{eS})} \left[\left(\frac{n}{n_0} \right)^\alpha - \left(\frac{n_S}{n_0} \right)^\alpha \right] \frac{T_{e0}}{e} \quad (21)$$

where

$$\alpha = \frac{\ln(T_{e0} / T_{eS})}{\ln(n_0 / n_S)} \quad (22)$$

The potential at the magnetic axis (where $n=n_0$) is

$$\varphi_0 = \frac{\ln(n_0 / n_S) + 1.71 \cdot \ln(T_{e0} / T_{eS})}{\ln(T_{e0} / T_{eS})} \cdot \frac{T_{e0} - T_{eS}}{e} \quad (23)$$

B. Toroidal velocity distribution

Using Eqs (15) and (21), we find the toroidal velocity:

$$v_T = -\frac{c}{B_p} \frac{d\varphi}{dr} = \frac{2c [\ln(n_0 / n_S) + 1.71 \cdot \ln(T_{e0} / T_{eS})] (T_{e0} - T_{eS})}{e B_{pS} a_S} \exp\left(-\frac{r^2}{a_S^2} \ln(T_{e0} / T_{eS})\right) \quad (24)$$

The corresponding angular frequency $\Omega = v_T / R_0$ is

$$\Omega = \frac{2c [\ln(n_0 / n_S) + 1.71 \cdot \ln(T_{e0} / T_{eS})] (T_{e0} - T_{eS})}{e B_{pS} a_S R_0} \exp\left(-\frac{r^2}{a_S^2} \ln(T_{e0} / T_{eS})\right) \quad (25)$$

The graphs of the angular frequency are presented in Fig. 2. We see that the rotation frequency $f = \Omega / 2\pi$ is maximum near the magnetic axis, where it is in the range of 10-15 kHz, and becomes smaller near the separatrix, where it is in the range of 1-1.5 kHz.

The radial shear, which in the "rectified" case is $\omega = R_0 d\Omega/dr$, is

$$\omega = \frac{4c \left[\ln(n_0/n_S) + 1.71 \cdot \ln(T_{e0}/T_{eS}) \right] \left[\ln(T_{e0}/T_{eS}) \right] (T_{e0} - T_{eS})}{eB_{PS} a_S^2} r \exp\left(-\frac{r^2}{a_S^2} \ln(T_{e0}/T_{eS})\right) \quad (26)$$

The maximum shear is

$$\omega_{\max} = \frac{4c \left[\ln(n_0/n_S) + 1.71 \cdot \ln(T_{e0}/T_{eS}) \right] \sqrt{\ln(T_{e0}/T_{eS})} (T_{e0} - T_{eS})}{eB_{PS} a_S^2 \sqrt{2e}} \quad (27)$$

The graphs of the radial shear normalized to the "Bohm frequency" $\omega_B = cT_{e0}/eB_{PS}a_T^2$ are presented in Fig. 3.

VI. DISCUSSION

The main assumption of our model is the assumption that the interior points of the confinement volume are connected to the walls along the field lines, which are very long in terms of the parallel heat loss but short in terms of the parallel electron equilibrium. In other words, our model is based on the hypothesis that the "disconnection" from the walls during the transition to a good confinement regime does not occur instantaneously, and the connection length does not jump from the finite value in a poor confinement mode to infinity in a good confinement mode, but rather increases gradually.

In the regime of the good confinement the concept of nested flux surfaces acquires a quantitative meaning, with the electron temperature and plasma density becoming flux functions to a high degree of accuracy. This, however, does not prevent the electrostatic potential from being translated from one flux surface to another along the field lines that connect them, Eq. (5). The potential distribution that follows from this model is expressed by Eq. (10).

The model predicts rotation velocity which is significantly smaller than the sound velocity c_s ; therefore, one should not expect any strong effect of the rotation on the

plasma equilibrium. On the other hand, the presence of the shear in the rotation frequency may have a stabilizing effect on drift instabilities which may be responsible for the plasma transport in the regimes of a “good” confinement. Indeed, the characteristic growth rate of most of the branches of the drift instability is typically less than [15]

$$\gamma \sim \frac{cT_e}{Ba_T^2} \quad (28)$$

A rough qualitative criterion of a significant stabilizing effect of the shear on the instability (used in the physics of a turbulent transport in tokamaks) is: $\omega > \gamma$ (see Ref. [16] for a survey). In the zone of the largest gradient of the electron temperature this condition is satisfied by a margin of 3 to 4 (Eq. (27) and Fig. 3). Therefore, one can expect a favorable effect of rotation on the plasma losses. As the shear in our model is associated with the gradient of the electron temperature (and, to a lesser degree, to the gradient of the plasma density), there is a possibility for the spontaneous formation of the transport barrier: the steepening of the temperature profile will increase a shear and give rise to a stronger suppression of the drift modes, thereby causing further reduction of the transport.

Note that steep temperature gradients have in some cases been observed at the SSPX facility (see, e.g., the lower panel in Fig. 7 of Ref. [4]). However, it would be premature to explain them by the mechanism of shear stabilization of drift modes, as they were probably associated with the chain of rather “fat” magnetic islands (see the upper two panels in Fig. 7 of Ref. [4]), and the gross change of the field line topology might be a more important factor in their formation. Direct measurements of plasma potential and/or plasma rotation would be needed to evaluate the role of shear-flow stabilization in this case.

The model works until the field lines are not too long. In the case of a spheromak, the upper bound on the field line length is determined by Eq. (7). Other factors that may limit the field line length are collisionless effects associated with Landau damping for the parallel motion. However, in the case of the SSPX spheromak (as well as other present-day spheromaks of a comparable size), the plasma is quite collisional, with the ratio N of the spheromak toroidal circumference $2\pi R$ to the Coulomb mean free path λ_{ei} being of order 1-4, depending on the temperature. This makes collisionless effects not very plausible.

On the other hand, if the regimes with significantly higher temperatures are reached in SSPX, various collisionless effects may become important, meaning that Eq. (10) will become invalid and direct relation between the local potential and local temperature and density will break down. Also, the condition of $L < L_2$ may break down. In these regimes, much more subtle effects would determine both the plasma potential distribution and the plasma rotation, the effects similar to those governing plasma rotation in tokamaks and largely related to the neoclassical effects (see Ref. [17] for an excellent survey).

Possible applicability of our model to reversed-field-pinches and field-reversed configurations would require additional analysis. It should also be remembered that our model is based on the hypothesis and plausibility arguments, not on the first-principle theory.

In the discussion of the plasma flow, we used assumption that the ion temperature is smaller than the electron temperature, and the forces associated with the non-uniformity of the magnetic field in the ion momentum equation (12) are negligible. For

$T_i \sim T_e$, the term $\sim T_i/a_s$ would have to be added to the RHS of Eq. (12). On the other hand, the electric force eE_n evaluated from Eq. (11) contains additional numerical factor $\sim 4-5$ compared to a simple estimate of T_e/a_s . Therefore, the $\text{grad}B$ force should not cause a significant change in our predictions for $T_i \sim T_e$. However, if T_i becomes a few times higher than T_e , our predictions regarding the rotation break down. This sets one more applicability limit for the present analysis.

Acknowledgments

The author is grateful to D.N. Hill, E.B. Hooper, H.S. McLean, C.A. Romero-Talamas, and R.D. Wood for fruitful discussions. Work performed under the auspices of the U.S. Department of Energy by University of California Lawrence Livermore National Laboratory under contract No. W-7405-Eng-48.

References

1. J.B. Taylor. "Relaxation and magnetic reconnection in plasmas." *Reviews of Modern Physics*, **58**, 741 (1986).
2. T.R. Jarboe. "Review of spheromak research." *Plasma Physics and Controlled Fusion*, **36**, 945 (1994).
3. H.S. McLean, S. Woodruff, E.B. Hooper, R.H. Bulmer, D.N. Hill, C. Holcomb, J. Moller, B.W. Stallard, R.D. Wood, Z. Wang. "Suppression of MHD fluctuations leading to improved confinement in a gun-driven spheromak." *Physical Review Letters*, **88**, 125004 (2002).
4. B.I. Cohen, E.B. Hooper, R.H. Cohen, D.N. Hill, H.S. McLean, R.D. Wood, S. Woodruff, C.R. Sovinec, G.A. Cone. "Simulation of spheromak evolution and energy confinement." *Physics of Plasmas*, **12**, 56106 (2005).
5. E.B. Hooper, T.A. Kopriva, B.I. Cohen, D.N. Hill, H.S. McLean, R.D. Wood, S. Woodruff, C.R. Sovinec. "Magnetic reconnection during flux conversion in a driven spheromak." *Physics of Plasmas*, **12**, 92503 (2005).
6. E.B. Hooper, R.H. Cohen, D.D. Ryutov. "Theory of edge plasma in a spheromak." *Journal of Nuclear Materials*, **278**, 104 (2000).
7. R.W. Moses, R.A. Gerwin, K.F. Schoenberg. "Transport implications of current drive by magnetic helicity injection." *Physics of Plasmas*, **8**, 4839 (2001).
8. J.M. Finn, C.R. Sovinec, D. del-Castillo-Negrete. "Chaotic scattering and self-organization in spheromak sustainment." *Physical Review Letters*, **85**, 4538 (2000).
9. C.R. Sovinec, J.M. Finn, D. del-Castillo-Negrete. "Formation and sustainment of electrostatically driven spheromaks in the resistive magnetohydrodynamic model." *Physics of Plasmas*, **8**, 475 (2001).
10. R.D. Wood, D.N. Hill, E.B. Hooper, S. Woodruff, H.S. McLean, B.W. Stallard. "Improved operation of the SSPX spheromak." *Nuclear Fusion*, **45**, 1582 (2005).
11. H.S. McLean, R.D. Wood, B.I. Cohen, E.B. Hooper, D.N. Hill, J.M. Moller, C. Romero-Talamas, S. Woodruff. "Transport and fluctuations in high temperature spheromak plasmas." *Physics of Plasmas*, **13**, 56105 (2006).
12. C.A. Romero-Talamas, C. Holcomb, P.M. Bellan, D.N. Hill. "Spheromak formation and sustainment studies at the sustained spheromak physics experiment using high-speed imaging and magnetic diagnostics." *Phys. Plasmas*, **13**, 022502 (2006).

13. C.T. Holcomb, T.R. Jarboe, D.N. Hill, S. Woodruff, R.D. Wood. "Sustained spheromak coaxial gun operation in the presence of an $n=1$ magnetic distortion." *Phys. Plasmas*, **13**, 022504 (2006).
14. S.I. Braginski. "Transport Processes in a Plasma." In: *Reviews of Plasma Physics*, v. 1, p. 205, M.A. Leontovich, Ed. (Consultants Bureau, NY, 1965).
15. A.B. Mikhailovskii. "Electromagnetic instabilities in an inhomogeneous plasma" (Institute of Physics, Bristol, 1992).
16. K.H. Burrell. "Effects of $E \times B$ velocity shear and magnetic shear on turbulence and transport in magnetic confinement devices," *Phys. Plasmas*, **4**, 1499 (1997).
17. K.C. Shaing. "Plasma Rotation in Tokamaks," International Tokamak Physics Activity (ITPA), Working Group on momentum transport/plasma rotation, April 24-27, 2006, Princeton, USA (private communication).

TABLE 1. Characteristic plasma parameters for SSPX

Spatial and temporal characteristics			Plasma parameters			Magnetic field (in the equatorial plane near the wall)	
R_0 , cm	a_S , cm	τ_{\perp} , ms	n , cm ⁻³	T_e , eV	Z_{eff}	B_T , kG	B_P , kG
25	25	0.3	10^{14}	100	2	3	3

TABLE 2. Some derived parameters for SSPX

ν_{ei} , s ⁻¹	λ_{ei} , cm	$N=2\pi R_0/\lambda_{ei}$	c_S , cm/s	ρ_i^* , cm
$3.5 \cdot 10^6$	150	1	$1.5 \cdot 10^7$	0.5

Figure captions

Fig. 1 The geometry of the problem. Shown is a set of flux surfaces for the toroidally-averaged magnetic field; O is the magnetic axis, R is the distance between the geometrical axis and a given point on a flux surface; R_0 is this parameter for the magnetic axis; a_s is a characteristic “radius” of the last-closed flux surface. In spheromaks, typically, $a_s \sim R_0$. Thick lines depict conducting walls of the flux conserver.

Fig. 2 The radial distribution of the rotation frequency [Eq. (25)] for $n_0/n_S = 2$, and $T_{eS} = 20 \text{ eV}$; central temperatures are indicated by the curves.

Fig. 3 The shear ω [Eq. (26)] normalized to the Bohm frequency $\omega_B = cT_{e0}/eB_{PS}a_T^2$ for $n_0/n_S = 2$, $T_{eS} = 20 \text{ eV}$, and the temperature at the magnetic axis $T_{e0} = 100 \text{ eV}$ (curve 1), 150 eV (curve 2), and 200 eV (curve 3). One sees that velocity shear exceeds the Bohm frequency over most of the plasma volume.

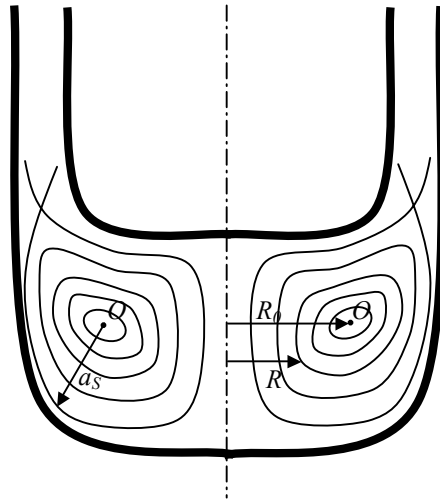


Fig. 1

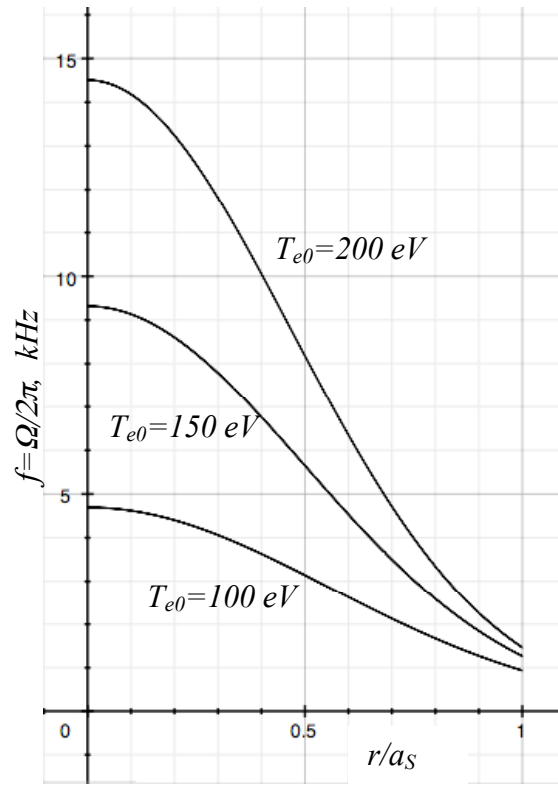


Fig. 2

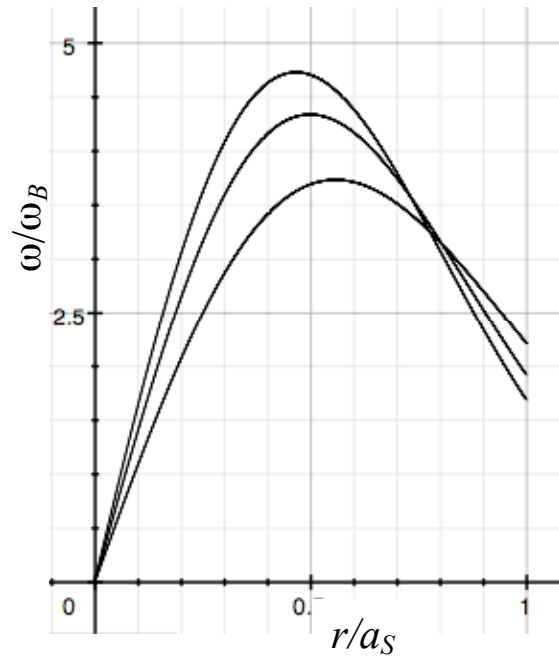


Fig. 3